diffusion-fundamentals.org

The Open-Access Journal for the Basic Principles of Diffusion Theory, Experiment and Application

Rapid Acquisition of NMR Diffusion-Diffraction *q*-Space Plots from Erythrocytes with Varying Gradient Orientation

Timothy J. Larkin,[1] *Guilhem Pages,*[1] *Allan M. Torres,*[2] *Philip W. Kuchel*[1]

[1] School of Molecular and Microbial Biosciences, University of Sydney, NSW 2006, Australia

[2] Nanoscale Organisation and Dynamics Group, University of Western Sydney, NSW, 2560, Australia

Corresponding author:
Philip W. Kuchel
School of Molecular and Microbial Biosciences
University of Sydney
NSW 2006, Australia
E-Mail: p.kuchel@mmb.usyd.edu.au

Abstract

The rapid-acquisition of *q*-space data from ^1H_2O undergoing restricted diffusion in suspensions of red blood cells (RBCs) is made possible using a recently implemented pulse sequence, where the phase cycling of the radio-frequency pulses is reduced by using unbalanced pairs of bipolar magnetic field-gradient pulses. The *q*-space plots obtained with this pulse sequence show a shift in the position of the first diffraction minimum when compared to data from classical pulsed field gradient stimulated echo experiments. Diffusion simulations were used to investigate the effect of the additional delay introduced by the bipolar gradient pulses on the form of the *q*-space plots. RBCs of normal discocyte shape align with an external magnetic field, and the angular dependence of *q*-space spectra from suspensions of RBCs was examined using a linear combination of gradients applied along the *y*- and *z*-axes. The resulting *q*-space plots showed a gradual disappearance of the first diffraction minimum as the angle at which the gradients were applied was changed from 0° (along the *z*-axis) to ~40°, beyond which the *q*-space plots showed no diffraction features. These experimental results were also evident in Monte-Carlo random walk simulations of diffusion in RBCs with field-gradients applied at varying angles with respect to cells aligned with $\mathbf{B}_0$.

Keywords: erythrocyte; diffusion-diffraction; Monte-Carlo; *q*-space; rapid-measurement of diffusion; red blood cell.

Abreviations: BSA, bovine serum albumin; NMR, nuclear magnetic resonance; PBS, phosphate buffered saline; PGSTE, pulsed field-gradient stimulated echo; RBC, red blood cell; SGP, short gradient pulse.

© 2009, P. W. Kuchel
diffusion-fundamentals.org 11 (2009) 67, pp 1-12

1. Introduction

The rapid-acquisition of diffusion-diffraction spectra from water diffusing in a suspension of red blood cells (RBCs) has been recently demonstrated [1], enabling the kinetic analysis of cell shape changes on the several-minute time scale. The method uses a pulse sequence developed by Pelta *et al.* [2], with a pair of unbalanced diffusion encoding bipolar gradient pulses (Fig. 1) to reduce the number of transients required per field gradient strength used. However, it was observed that by using this rapid-acquisition pulse sequence a shift occurred in the position of the diffraction minima to higher q values when compared with data from the classical pulsed field-gradient stimulated echo (PGSTE) diffusion experiment (Fig. 2).

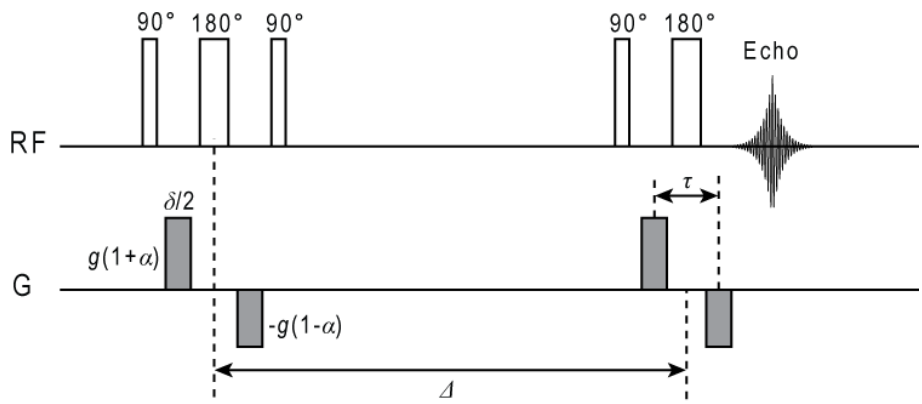

Fig. 1: Rapid-acquisition diffusion pulse sequence of Pelta *et al.* [2] which uses unbalanced pairs of bipolar gradient pulses. RF refers to the time train of the radiofrequency pulses, while G refers to the field gradient pulse time train. Δ is the diffusion time, δ is the gradient duration, τ is the time between the midpoints of the antiphase field gradient pulses, g is the gradient amplitude, and α is the unbalancing factor.

Diffusion-measuring nuclear magnetic resonance (NMR) spectroscopy encodes spatial information in the phase of nuclear spins through the application of magnetic field gradient pulses. Translational displacement between a pair of gradient pulses can then be measured, and hence diffusion coefficients calculated [3]. A geometry that restricts diffusion can result in spatial coherences of the magnetisation phases in the sample, giving rise to interference and diffraction-like effects in the data. These effects termed 'diffusion-coherence' [4, 5] are readily observed by plotting normalised signal intensity versus the spatial wave-number vector **q** (units, m^{-1}):

$$\mathbf{q} = (2\pi)^{-1} \gamma \delta \mathbf{g} \tag{1}$$

where γ is the magnetogyric ratio, δ is the duration of the magnetic field-gradient pulses applied during the experiment, and **g** is the magnetic field-gradient vector.

PGSTE experiments on the diffusion of water in suspensions of RBCs produce q-space plots with several well-defined features (Fig. 2); these arise because the cells align in the

uniform magnetic field [5, 6]. The first feature is a shoulder due to water 'hopping' between the pore-like spaces between the cells as it diffuses in the extracellular medium, followed by several diffraction minima arising from water undergoing restricted diffusion inside the cells [7]. The position of diffraction minima in *q*-space plots reports on the amplitude of the average propagator, and hence on the size of the restricting geometry; this average propagator is calculated by taking the Fourier transform of the *q*-space data [8, 9].The features of the calculated average propagator can be enhanced by the use of a digital filter, followed by application of the second derivative to suppress both the strong initial signal, and the noise at high *q*-values [8].

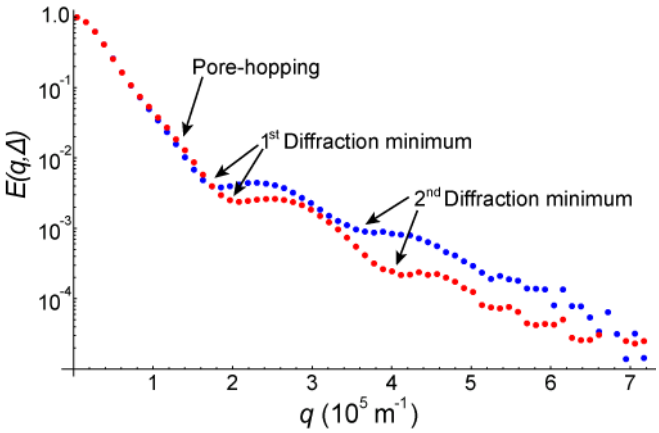

Fig. 2: Comparison of *q*-space plots obtained using the classical (blue) and rapid-acquisition PGSTE (red) pulse sequences from a suspension of human RBCs. The positions of the important coherence features are shown. We can note a shift in the minimum positions between both pulse sequences. The experimental details are described in the text.

Under conditions where the short gradient-pulse (SGP) approximation is not valid, the position of diffraction minima are dependent on the duration of the gradient pulses relative to the time interval over which diffusion is measured [10, 11]. Therefore, we hypothesised that the shift in the position of the minima is introduced by using bipolar gradient pulses. To test this idea we conducted Monte-Carlo random walk simulations of diffusion in RBCs with varying separation of the bipolar pulses.

We also aimed to explore a new application of the rapid-acquisition PGSTE sequence to generate *q*-space plots at varying angles across a sample of RBCs, and correlate these real data with simulations of diffusion in RBCs with variable orientation.

2. Experimental

Fresh blood was obtained from a healthy donor (TJL); the RBCs were isolated by centrifugation at 3000 × *g* for 10 min at 4°C, followed by aspiration of the plasma and buffy coat. The RBCs were then washed three times in isotonic phosphate buffered saline (PBS), by centrifugation as just described, and bubbled for 15 min with CO to render the haemoglobin diamagnetic. The cells were suspended in isotonic PBS containing 0.5%

(w/v) bovine serum albumin (BSA) and 10 mM glucose, to give a final haematocrit (H_t) of 70%.

The NMR experiments were carried out on a Bruker Avance 500 WB spectrometer equipped with a micro-imaging probe capable of producing gradients of 3 T m^{-1} along the *x*-, *y*- and *z*-axes. The sample of RBCs was placed in a 5-mm Shigemi tube and height restricted to 1 cm to ensure that the sample was in the constant-gradient region of the probe. The experiments were performed at 25°C using the optimised fast diffusion pulse sequence [1]. The diffusion time Δ was 20 ms, δ was 4 ms, the gradient recovery delay (τ-$\delta/2$) was 1 ms, and the gradient unbalancing factor α was set to 0.3. Gradients were applied at 0° (along the *z*-axis), 2°, 5°, 8°, 10°, 15°, 20°, 30°, 40°, 45°, 50°, 60°, 70°, 80°, and 90° (along the *y*-axis), using a combination of *z*- and *y*- gradients, with each *q*-space plot using 64 linearly-spaced gradient values.

3. Simulations of restricted Diffusion in RBCs

The Monte-Carlo random walk simulation of the diffusion of water in a suspension of RBCs was performed using programs written in a combination of *Mathematica* 6.0 (Wolfram, Champaign, IL) and C. *Mathematica* has a library of C functions for communication with an external C program, which allow for more efficient execution of the simulations. During each time step (t) of the simulation, the diffusing particle was moved one jump length (s), in the *x*-, *y*- and *z*-directions, where s was calculated from the diffusion coefficient (D) and the Einstein equation [12]:

$$s = \sqrt{2Dt} \tag{2}$$

The direction of the jump along each axis, either $\pm s$, was determined using a binary digit randomly generated with the function Random in *Mathematica*.

The unit cell for the simulations was based on that described previously [13-16], consisting of a discocyte-shaped RBC inside a hexagonal prism (Fig. 3a), which allows the transmembrane exchange of water to be included by applying periodic boundary conditions at the prism surface. The RBC surface was described by the equation [17],

$$\left(X^2 + Y^2 + Z^2\right)^2 + P\left(Y^2 + Z^2\right) + Q\left(X\right)^2 + R = 0 \tag{3}$$

P, Q and R are constants related to the dimensions of the RBC, a the maximum thickness, b the minimum thickness, and d the main diameter (Fig 3b). Thus,

$$\begin{aligned} P &= -\frac{d^2}{2} + \frac{a^2}{2}\left(\frac{d^2}{b^2} - 1\right)\left(1 - \frac{b^2}{a^2}\right)^{1/2} \\ Q &= \frac{d^2}{b^2}P + \frac{b^2}{4}\left(\frac{d^4}{b^4} - 1\right) \\ R &= -\frac{d^2}{4}P - \frac{d^4}{16} \end{aligned} \tag{4}$$

In Eq. 3 X, Y and Z represent the modified Cartesian coordinates,

$$\begin{aligned} X &= z\sin\theta + \cos\theta\left(x\cos\psi - y\sin\psi\right) \\ Y &= y\cos\psi + x\sin\psi \\ Z &= z\cos\theta - \sin\theta\left(x\cos\psi - y\sin\psi\right) \end{aligned} \tag{5}$$

so rotation of the body about the *y*- and *z*-axes by θ and ψ (Fig 3c), respectively, can be readily included in the simulations. Rotation of the cell about the *y*-axis allows the orientation of the cell with respect to $\mathbf{B}_0$ to be varied, however, in all the simulations described here the cells were aligned with $\mathbf{B}_0$ (by definition along the *z*-axis), therefore θ was fixed at 0°. While RBCs align with an external magnetic field, they will adopt random orientations in the *x*/*y*-plane, and rotating the cell about the *z*-axis allows this to be included in the simulations.

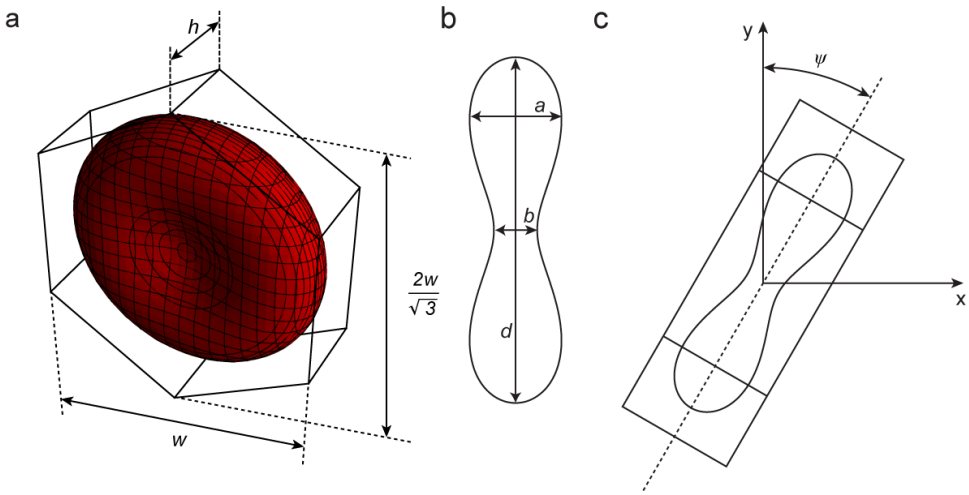

Fig. 3: a Schematic of the unit cell used in the diffusion simulations, consisting of an RBC inside a hexagonal prism. The dimensions of the prism are shown with *w* being the width, and *h* the depth of the prism; **b** shows a cross section through the model RBC used for the simulations, *a* is the maximum thickness of the cell, *b* is the minimum thickness, and *d* is the main diameter; and **c** illustrates the definition of ψ, the rotation angle about the z-axis.

The dimensions of the hexagonal prism, which was also rotatable about the *y*- and *z*-axes, were determined by fixing the volume of the prism (V_{prism}) with respect to the volume of the cell (V_{cell}),

$$V_{\text{prism}} = V_{\text{cell}} / H_t \tag{6}$$

where H_t is the hematocrit content and V_{prism} is given by,

$$V_{\text{prism}} = w^2 h \sin\left(\pi/3\right) \tag{7}$$

As the RBC membrane is semi-permeable to water, there are two possible outcomes if a jump would take a particle across the cell boundary; the particle could transit the

membrane or be reflected at the boundary. The probability (t_p) of a particle transitioning the membrane is calculated using the relationship [13],

$$t_p = P_d s_{in/out} / D_{in/out} \tag{8}$$

where P_d is the membrane permeability to water, and $s_{in/out}$ and $D_{in/out}$ are the jump length and diffusion coefficient of the particle either inside or outside the RBC, respectively. Reflection of a particle at the boundary requires the solution of the intersection of a line with the surface describing the RBC. The coefficients of the resulting quartic equation were calculated using *Mathematica* (See Appendix).

Each spin acquires an additional phase angle (φ) during the gradient pulses of the PGSTE experiment, dependent on its spatial position, and the magnitude of the magnetic field gradient pulse (g). This acquired phase angle is implemented in a Monte-Carlo random walk simulation by updating the value of φ after each jump using the equation,

$$\varphi(g) = \gamma g t |\mathbf{r}| \tag{9}$$

where t is the duration of a jump, and $|\mathbf{r}|$ is the magnitude of the position vector of the particle with respect to the applied gradient. During the first gradient pulse, phase is accumulated (positive g), while during the second gradient pulse g has the opposite sign. The effect of the 180° RF pulses in the bipolar gradient pulses was ignored, with the first pair of pulses having positive g, and the second pair negative g. The accumulated phase angle at the end of the simulation is converted into a signal intensity (E) by taking the projection of the magnetisation vector onto the $-y$-axis, using the expression:

$$E(g) = \cos(\varphi) g \tag{10}$$

The first set of simulations were based on the rapid-acquisition pulse sequence shown in Fig. 1, using the experimental parameters used to acquire real q-space plots from suspensions of RBCs [1]. Specifically, these were Δ = 20 ms, δ = 3 ms, α = 0.3, and gradient recovery delays of 0, 1 and 2 ms, to investigate the effect of this delay on the position of the first diffraction minimum. With a gradient-recovery delay of 0 ms the pulse sequence is equivalent to the classical PGSTE pulse sequence; but a simulation using unbalanced pairs of gradient pulses with δ = 3 ms was run to determine the effect on the shape of q-space plots. The last simulation in this set used the rapid-acquisition pulse sequence with the parameters that were used to conduct the real experiment in which the gradient angles were varied, namely Δ = 20 ms, δ = 4 ms, α = 0.3, and a gradient recovery delay of 1 ms.

The second set of simulations involved changing the orientation of the magnetic field-gradients across aligned RBCs, using a combination of gradients along the z- and y-axes. These simulations used the classical PGSTE pulse sequence with Δ = 20 ms, δ = 2 ms, and gradient orientations as described in the experimental section. For both sets of simulations the dimensions of the RBCs were a = 2.12 μm, b = 1 μm, and d = 8 μm, which gives a model RBC with the mean volume of human RBCs of 86 fL [18]. The membrane permeability was set to the literature value for human RBCs at 25°C of 6.1×10^{-5} ms^{-1} [19]. The magnetogyric ratio of ^{1}H, 2.62752×10^8 rad s^{-1}T^{-1} was used, and the magnetic field gradient (g) was varied along the z-axis in a 96 step arithmetic series between 0 and 10 T m^{-1}. One million particle trajectories were used for each simulation, being divided into packets of 1000 trajectories. For each packet a rotation about the z-axis by the angle ψ was applied in steps of 0.18°, giving a total rotation of the cell of 180°, to

generate the varying orientations expected in a real RBC sample. The signal attenuation data obtained from the simulations were interpolated in *Mathematica* to give 1000 points, using a shifting cubic spline prior to plotting the logarithmic ordinate to enhance visualisation of the coherence features.

The mean length of a chord along the *z*-axis for cells oriented at differing angles with respect to $\mathbf{B}_0$ was determined by randomly generating 10^5 points inside the cell and calculating the length of the chord parallel to the *z*-axis though each point. For comparison purposes the mean length of a chord along the *z*-axis was also calculated for an oblate spheroid that was oriented at various angles to $\mathbf{B}_0$. The radii of the spheroid were 4 μm and 1.28 μm, giving a volume of ~86 fL.

4. Results and Discussion

The implementation of the rapid-measurement diffusion pulse sequence simulation was tested by performing simulations of free diffusion using the diffusion coefficient of water at 25°C of 2.30×10^{-9} m^2s^{-1}, $\Delta = 20$ ms and several values of δ, α and τ. The fitting of the resultant signal decays using the equation of Pelta *et al.* [2] consistently yielded a diffusion coefficient of 2.39×10^{-9} m^2s^{-1}. Therefore the equation describing the signal decay was derived using the *Mathematica* program described by Momot and Kuchel [20], and found to be different from the one published in [2],

$$\frac{I_g}{I_0} = \exp\left\{-D\gamma^2 g^2 \delta^2 \left[\Delta - \delta\left(\alpha^2+1\right)/12 - \tau\left(1-\alpha^2\right)/2\right]\right\} \tag{11}$$

When this new equation was fitted to the signal decays the expected diffusion coefficient of 2.30×10^{-9} m^2s^{-1} was obtained.

q-Space plots for simulations of water diffusing in RBCs using the rapid-acquisition pulse sequence with gradient recovery times of 0, 1 and 2 ms are shown in Fig. 4. The curves show a systematic shift in the position of the first diffraction minimum towards higher *q* values as the delay is increased; this correlates well with the observed shift seen in real experimental data (Fig. 2). The position of the first diffraction minimum in the real data obtained using PGSTE and the rapid-acquisition pulse sequences were 1.9×10^5 m^{-1} and 2.0×10^5 m^{-1} (gradient recovery between bipolar pulses = 2 ms), respectively, while from the Monte-Carlo simulations with the same parameters, the minima appeared at 1.6×10^5 m^{-1} and 1.8×10^5 m^{-1}, respectively. This represents a difference in the apparent mean-displacement of water between the simulated and real data, with a larger apparent displacement in the simulated data. We conclude that the source of the difference was the assumption of an infinitely thin membrane used in the simulations.

The position of the first minimum was identical in the simulated data obtained using the rapid-acquisition with no gradient-recovery delay, and the classical PGSTE with $\delta = 3$ms, and therefore we concluded that the source of the shift in the experimental data was from the non-negligible diffusion that occurs during the delay introduced by the bipolar gradient pulses, and was not due to the unbalancing of the gradient pulses, *per se*.

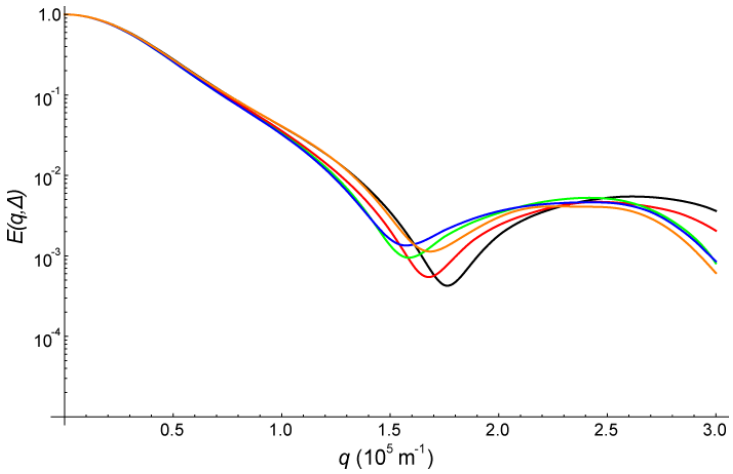

Fig. 4: Simulated q-space plots of water diffusing in RBCs comparing results from the classical PGSTE pulse sequence with δ = 3 ms (blue) with results from the rapid-acquisition pulse sequence with δ = 3 ms, and gradient recovery delays (δ-τ) of 2 ms (black), 1 ms (red), and 0 ms (green). Shown in orange is a q-space plot from a simulation with δ = 4 ms and a gradient recovery delay of 1 ms (experimental conditions used for the gradient orientation study).

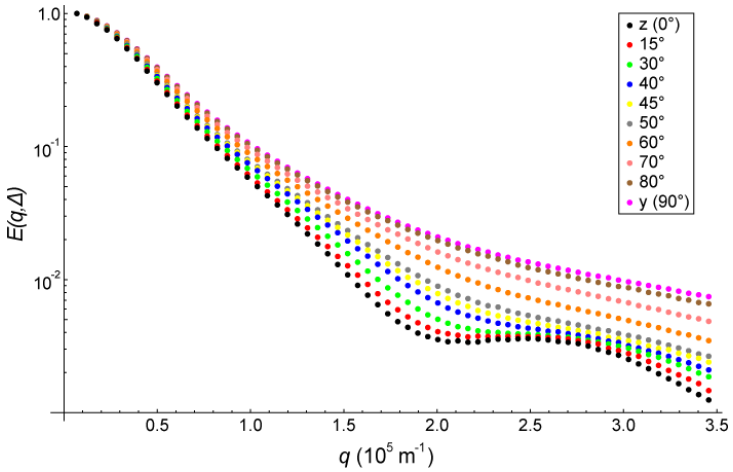

Fig. 5: q-Space plots from a real suspension of RBCs where magnetic field-gradients were applied at various angles across the cells using combinations of y- and z-axis gradients. Data were acquired for gradients at several angles between 0° and 30°, however, for clarity only the data for 15° are shown in this domain.

q-Space plots generated from real experiments with the rapid-acquisition sequence, where the angle of the gradients across a suspension of RBCs was varied, are shown in Fig. 5. As the angle of the gradients was increased there was a gradual broadening and shift in the position of the first diffraction minimum towards higher values of q, with the feature being lost in the region of 40-45°. The data obtained for gradients between 0° and 30° were overlapping, and for clarity only the data for 15° are shown in the graph. The gradual shift in the diffraction minimum in samples of RBCs contrasts with experimental

data obtained from diffusion in orientated cylinders with large length-to-radius ratio [21, 22], where the coherence features were lost after a rotation of only a few degrees.
The corresponding data from simulations of diffusion performed on cells orientated with the magnetic field where the gradients were applied at various angles (Fig. 6), showed the loss of the first diffraction minimum for gradient orientations greater than ~45°. The shift in the position of the diffraction minimum was also more pronounced in the simulated plots, with the minima in the real experimental data being broader and shallower than those observed for simulated data. The broadening seen in the real experimental data is, in part, a consequence of the distribution of cell sizes that is normal for real blood samples [23], giving a range of mean displacements along the gradient axis. Such a variation of cell size was not considered in the simulations where all the cells had the same dimensions.

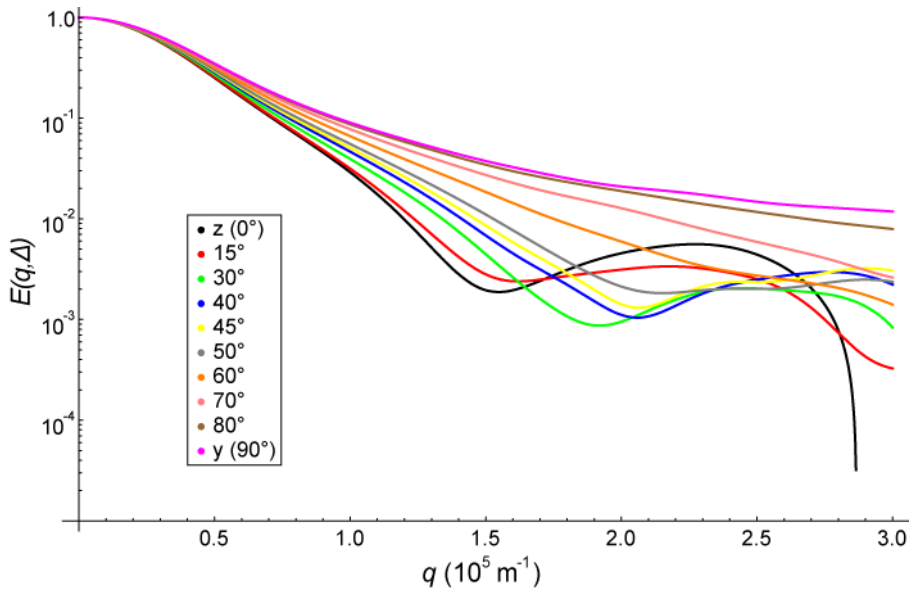

Fig. 6: Simulated *q*-space plots for RBCs with variable gradient orientation angles relative to the aligned cells. The gradient angles and respective colours are identical to those in Fig 5. All curves were generated using the pulse-timing of the classical PGSTE pulse sequence and combinations of gradients along the *y*- and *z*-axes.

Simulated *q*-space plots for RBCs oriented at 0°, 45° and 90° to the magnetic field have been reported previously [24], but the cells were approximated by a flat cylinder. Nevertheless there is good agreement with the position of the previous diffraction minima [24] with our simulated data presented here, our diffraction minima are significantly broader however. The additional rotation of the cell about the *z*-axis creates a range of cell profiles along the *y*-axis, broadening the minima in *q*-space plots from our simulated data.

The gradual shift and then disappearance of the first diffraction minimum observed in the experimental data can be explained by the curved profile of an RBC that is aligned with $\mathbf{B}_0$, as shown in Fig. 3b. Small changes in the orientation of the gradients (or of the cells) can be expected to result in only a small reduction in the profile of the cell that is projected along the gradient axis. This is demonstrated in Fig. 7, where the mean chord-length projected along the *z*-axis of an orientated cell, or oblate spheroid, is seen to decline slowly until an orientation of ~10°; this is followed by a rapid change to ~45°, after which the mean chord-length reaches a plateau. The plateau in mean chord-length for orientations greater than 45° corresponds well with the loss of the first diffraction minimum that was seen in the experimental and simulated data.

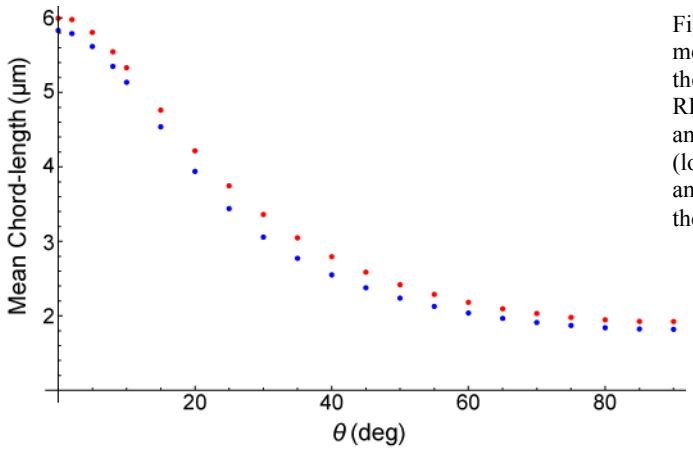

Fig. **7.** Variation of the mean length of a chord in the *z*-direction of a model RBC (Fig. 3, upper points), and an oblate spheroid (lower points), with the angle of orientation (θ) of the cell with respect to $\mathbf{B}_0$

5. Conclusions

We investigated the source of the shift in the position of the diffraction minima in *q*-space plots from water undergoing restricted diffusion in RBC suspensions when using a rapid-acquisition PGSTE pulse sequence. The delay introduced into the pulse sequence by the use of bipolar gradient pulses is the cause. We also used this pulse sequence to acquire *q*-space plots from real experiments on RBC suspensions where the field gradients had various angles relative to $\mathbf{B}_0$, and compared these with simulated *q*-space plots from orientated RBCs. The demonstrated dependence of the form of a *q*-space plot on the choice of NMR pulse sequence is an important factor to be considered in deriving estimates of the main diameter of RBCs from *q*-space data.

6. Acknowledgements

The work was funded by a Discovery Project Grant from the Australian Research Council to PWK. TJL received a University of Sydney Postgraduate Award. Dr Bob Chapman is thanked for valuable NMR-software developments and discussions, and Professor Bill Price for generously providing access to the 500 MHz-wb NMR spectrometer at the University of Western Sydney.

7. Appendix

The following is taken from a *Mathematica* program used to derive the coefficients of the quartic equation describing the intersection of a line with the surface describing the RBC.

```
(* Parametric equation of the line between the points {x1,y1,z1} and {x2,y2,z2} *)
x = x1 + t (x2 - x1);
y = y1 + t (y2 - y1);
z = z1 + t (z2 - z1);

(* Equation that describes the RBC surface *)
eqn = ((z Sin[θ] + Cos[θ] (x Cos[ψ] - y Sin[ψ]))^2 +
      (y Cos[ψ] + x Sin[ψ])^2 + (z Cos[θ] - Sin[θ] (x Cos[ψ] - y Sin[ψ]))^2)^2 +
   P ((y Cos[ψ] + x Sin[ψ])^2 + (z Cos[θ] - Sin[θ] (x Cos[ψ] - y Sin[ψ]))^2) +
   Q ((z Sin[θ] + Cos[θ] (x Cos[ψ] - y Sin[ψ]))^2) + R;

(* The solution for the intersection point is found by substituting the
 parametric equation of the line into the equation describing the RBC surface *)
soln = Collect[Expand[eqn], t];

(* The variable soln now contains the terms of a quartic equation
 in t. Each coeffient of t can then be extracted and simplified *)
(* The t^4 term is *)
FullSimplify[soln[[-1]]]
```

$$t^4 \left((x1-x2)^2+(y1-y2)^2+(z1-z2)^2\right)^2$$

```
(* The t^3 term is *)
FullSimplify[soln[[-2]]]
```

$$-4\,t^3 \left(x1^2-x1\,x2+y1^2-y1\,y2+z1\,(z1-z2)\right)\left((x1-x2)^2+(y1-y2)^2+(z1-z2)^2\right)$$

```
(* The t^2 term is *)
FullSimplify[soln[[-3]]]
```

$$\begin{aligned}
&\frac{1}{4}\,t^2 \Big(Q\left((x1-x2)^2+(y1-y2)^2+2\,(z1-z2)^2\right)+P\left(3\,(x1-x2)^2+3\,(y1-y2)^2+2\,(z1-z2)^2\right)+\\
&\quad 8\Big(3\,x1^4-6\,x1^3\,x2+3\,y1^4-6\,y1^3\,y2+x2^2\left(y1^2+z1^2\right)+z1^2\left(y2^2+3\,(z1-z2)^2\right)+\\
&\qquad 2\,y1\,y2\,z1\,(-3\,z1+2\,z2)+x1^2\left(3\,x2^2+6\,y1^2-6\,y1\,y2+y2^2+6\,z1^2-6\,z1\,z2+z2^2\right)+\\
&\qquad y1^2\left(3\,y2^2+6\,z1^2-6\,z1\,z2+z2^2\right)+2\,x1\,x2\left(-3\,y1^2+2\,y1\,y2+z1\,(-3\,z1+2\,z2)\right)\Big)-\\
&\quad (P-Q)\Big(\Big((x1-x2)^2+(y1-y2)^2-2\,(z1-z2)^2\Big)\,\mathrm{Cos}[2\,\theta]+\\
&\qquad 2\Big(2\,(z1-z2)\,\mathrm{Sin}[2\,\theta]\,\big((x1-x2)\,\mathrm{Cos}[\psi]+(-y1+y2)\,\mathrm{Sin}[\psi]\big)+\\
&\qquad\quad \mathrm{Cos}[\theta]^2\Big(\Big((x1-x2)^2-(y1-y2)^2\Big)\,\mathrm{Cos}[2\,\psi]-2\,(x1-x2)\,(y1-y2)\,\mathrm{Sin}[2\,\psi]\Big)\Big)\Big)\Big)
\end{aligned}$$

```
(* The t term is *)
FullSimplify[soln[[-4]]]
```

$$\begin{aligned}
&\frac{1}{2}\,t\Big(-8\left(x1^2+y1^2+z1^2\right)\left(x1^2-x1\,x2+y1^2-y1\,y2+z1\,(z1-z2)\right)-\\
&\quad Q\left(x1^2-x1\,x2+y1^2-y1\,y2+2\,z1\,(z1-z2)\right)+P\,(3\,x1\,(-x1+x2)+3\,y1\,(-y1+y2)+2\,z1\,(-z1+z2))+\\
&\quad (P-Q)\Big(\left(x1^2-x1\,x2+y1^2-y1\,y2+2\,z1\,(-z1+z2)\right)\mathrm{Cos}[2\,\theta]+\\
&\qquad 2\Big(\mathrm{Sin}[2\,\theta]\,\big((2\,x1\,z1-x2\,z1-x1\,z2)\,\mathrm{Cos}[\psi]+(y2\,z1+y1\,(-2\,z1+z2))\,\mathrm{Sin}[\psi]\big)+\\
&\qquad\quad \mathrm{Cos}[\theta]^2\Big(\left(x1^2-x1\,x2+y1\,(-y1+y2)\right)\mathrm{Cos}[2\,\psi]+(x2\,y1+x1\,(-2\,y1+y2))\,\mathrm{Sin}[2\,\psi]\Big)\Big)\Big)\Big)
\end{aligned}$$

```
(* The constant term is *)
FullSimplify[Drop[soln, -4]]
```

$$\begin{aligned}
&\frac{1}{4}\Big(4\,R+3\,P\left(x1^2+y1^2\right)+2\,P\,z1^2+4\left(x1^2+y1^2+z1^2\right)^2+\\
&\quad Q\left(x1^2+y1^2+2\,z1^2\right)-(P-Q)\Big(\left(x1^2+y1^2-2\,z1^2\right)\mathrm{Cos}[2\,\theta]+\\
&\qquad 4\,z1\,\mathrm{Sin}[2\,\theta]\,(x1\,\mathrm{Cos}[\psi]-y1\,\mathrm{Sin}[\psi])+2\,\mathrm{Cos}[\theta]^2\left(\left(x1^2-y1^2\right)\mathrm{Cos}[2\,\psi]-2\,x1\,y1\,\mathrm{Sin}[2\,\psi]\right)\Big)\Big)
\end{aligned}$$

The intersection was determined by substitution of the coordinates of the points inside and outside the RBC surface, and then using the *Mathematica* function Solve to calculate the roots of the quartic. Substitution of the real root in the interval (0,1) into the parametric equation of the line then yielded the coordinates of the intersection point.

8. References

[1] G. Pages, D. Szekely, P. W. Kuchel. J. Magn. Reson. Imag. 28 (2008) 1409-1416.
[2] M. D. Pelta, G. A. Morris, M. J. Stchedroff, S. J. Hammond. Magn. Reson. Chem. 40 (2002) S147-S152.
[3] E. O. Stejskal, J. E. Tanner. J. Chem. Phys. 42 (1965) 288-292.
[4] P. T. Callaghan, A. Coy, D. Macgowan, K. J. Packer, F. O. Zelaya. Nature 351 (1991) 467-469.
[5] P. W. Kuchel, A. Coy, P. Stilbs. Magn. Reson. Med. 37 (1997) 637-643.
[6] P. W. Kuchel, C. J. Durrant, B. E. Chapman, P. S. Jarrett, D. G. Regan. J. Magn. Reson. 145 (2000) 291-301.
[7] A. M. Torres, A. T. Taurins, D. G. Regan, B. E. Chapman, P. W. Kuchel. J. Magn. Reson. 138 (1999) 135-143.
[8] P. W. Kuchel, T. R. Eykyn, D. G. Regan. Magn. Reson. Med. 52 (2004) 907-912.
[9] J. Kärger, W. Heink. J. Magn. Reson. 51 (1983) 1-7.
[10] P. Linse, O. Soderman. J. Magn. Reson. A 116 (1995) 77-86.
[11] W. S. Price, P. Stilbs, O. Soderman. J. Magn. Reson. 160 (2003) 139-143.
[12] A. Einstein. Annalen der Physik 17 (1905) 549-560.
[13] D. G. Regan, P. W. Kuchel. Eur. Biophys. J. 29 (2000) 221-227.
[14] D. G. Regan, P. W. Kuchel. Biophys. J. 83 (2002) 161-171.
[15] D. G. Regan, P. W. Kuchel. Eur. Biophys. J. 32 (2003) 671-675.
[16] D. G. Regan, P. W. Kuchel. Eur. Biophys. J. 31 (2003) 563-574.
[17] P. W. Kuchel, E. D. Fackerell. Bull. Math. Biol. 61 (1999) 209-220.
[18] J. V. Dacie, S. M. Lewis. 1975. Practical Haematology. Churchill Livingstone, Edinburgh.
[19] G. Benga, V. I. Pop, O. Popescu, V. Borza. J. Biochem. Biophys. Methods 21 (1990) 87-102.
[20] K. I. Momot, P. W. Kuchel. Concepts Magn. Reson. 28A (2006) 249-269.
[21] L. Avram, Y. Assaf, Y. Cohen. J. Magn. Reson. 169 (2004) 30-38.
[22] L. Avram, E. Ozarslan, Y. Assaf, A. Bar-Shir, Y. Cohen, P. J. Basser. NMR Biomed. 21 (2008) 888-898.
[23] C. Price-Jones, J. M. Vaughan, H. M. Goddard. J. Pathol. Bacteriol. 40 (1935) 503-519.
[24] P. C. Jiang, T. Y. Yu, W. C. Perng, L. P. Hwang. Biophys. J. 80 (2001) 2493-2504.